Poster Contributions

https://doi.org/10.1017/S1743921318007135 Published online by Cambridge University Press

Dwarf Galaxies: From the Deep Universe to the Present
Proceedings IAU Symposium No. 344, 2019
K. B. W. McQuinn & S. Stierwalt, eds.

doi:10.1017/S1743921318007135

Exploring 3D data of Dwarf Galaxies

Katarzyna Bensch, Christina Thöne, Antonio de Ugarte Postigo, Luca Izzo and David Alexander Kann

Instituto de Astrofísica de Andalucía,
Glorieta de la Astronomía s/n, 18008, Granada, Spain
email: kasia@iaa.es

Abstract. Dwarf irregular galaxies are places of ongoing star-formation in the low-redshift Universe. Low metallicity dwarfs were originally thought to be the youngest galaxies in the local Universe, however, there is now evidence that they consist of matter which has previously undergone evolution and is enriched by star-formation. Here we present a sample of seven nearby metal-poor dwarf galaxies with a young stellar populations selected from the SDSS which we study using integral field unit (IFU) data from the VIMOS instrument, covering the spectral range between the He II 4686 line and the [SII] 6718/6733 Å doublet. We present property maps across the galaxies and compare different galaxies and different HII regions within the same galaxy. We find that the properties within one galaxy are not uniform and they also differ between different galaxies concerning star-formation, kinematics and metallicity and morphology. The observed differences across individual galaxies together with disturbed kinematics and morphologies can be interpreted as possible signs of recent interactions and/or mergers. Additionally, we present a comparison of different metallicity calibrations and search for systematic differences obtained using different methods.

Keywords. Dwarf galaxies, Star-formation, Evolution, IFU

1. Introduction

Dwarf galaxies are great laboratories to study star-formation (SF) in the local Universe. Observations show that most of the SF in the nearby Universe takes place in dwarf irregulars and blue compact galaxies (e.g. Cowie *et al.* 1996). The star-formation rate (SFR) space-time variations in late-type dwarf galaxies (Dohm-Palmer *et al.* 1998, Dohm-Palmer *et al.* 2002) seem to be consistent with the prediction of stochastic self-propagating star-formation (Seiden *et al.* 1979) where in different regions over periods of several hundred million years SF is turning on and off. The comparison of different evolutionary scenarios presented by Martín-Manjón *et al.* (2012) favoured a bursting SF model where stars are formed in intense SF bursts with long quiescent periods inbetween (Davies & Phillipps 1988; Bradamante, Matteucci & D'Ercole 1998).

Previous studies suggest that dwarfs are not necessarily a distinct type of galaxies (Mateo 1998). A comparison between different galaxy types of varying sizes showed a continuous transition in structural, kinematic and stellar population features (Tolstoy *et al.* 2009). Nevertheless, it is still somewhat unclear whether irregular dwarf galaxies are genuinely young galaxies or whether their evolution is simply different compared to large galaxies. Originally, it was thought that dwarf galaxies were recently formed from pristine HI clouds. However, dwarf galaxies with an underlying older population have been found, which leads us to think they are actually older galaxies with recent new bursts of SF (Papaderos *et al.* 1996). The reason for their low metallicity would lie in their low gravitational potential that is not able to retain enriched gas.

Large surveys such as the SDSS Abazajian *et al.* (2005) have led to the detection of many dwarf galaxies. These large samples are great sources of global galaxy properties, however, they may give erroneous conclusions about their formation and evolution, since the properties vary across the galaxy. We therefore need resolved information that reflects the variations across individual galaxies. The main goal of this work is to perform detailed, resolved studies of individual star-forming regions in different dwarf galaxies in order to study their SF histories and chemical evolution and the interplay between these factors.

2. Sample selection, observations and analysis

Our sample consists of seven metal-poor dwarf irregular galaxies selected from SDSS DR3 spectroscopy survey with the following selection criteria: (1) Low metallicity, $12 + \log(\mathrm{O/H}) < 8.0$; (2) equivalent width (EW) of H$\beta > 30$ Å (implying that the galaxy is dominated by a young stellar population); and (3) a visibly extended structure of the galaxy consisting of several star-forming regions. The dwarf galaxies presented in this work have been observed with the VIsible Multi-Object Spectrograph (VIMOS, Le Févre *et al.* 2003) instrument at the ESO/VLT. All the targets have been observed with the Integral Field Unit mode and the high-resolution BLUE grism, covering the wavelength range between 3700 and 5200 Å with a dispersion of 0.57 Å/pixel, and the ORANGE grism, with a coverage between 5250 and 7400 Å with a dispersion of 0.6 Å/pixel.

Using our own IDL codes we extracted maps of emission lines and other properties of the galaxy from the VIMOS/IFU cubes. To obtain emission-line fluxes we sum the flux in the spectral direction around the redshifted position of each emission line for each spaxel and subtract the galaxy continuum. To extract integrated spectra of individual star-forming regions we use a modified PYTHON code based on the H II explorer algorithm that automatically finds individual HII regions using Hα emission maps (Sanchez *et al.* 2012). After extraction we analyse those spectra using the IRAF SPLOT package to measure emission-line fluxes.

3. Results

3.1. *Metallicity of star-forming regions*

To determine the metallicities of HII regions we used the Python code pyMCZ Bianco *et al.* (2016) that determines the statistical oxygen abundance confidence region via Monte Carlo simulations for several strong emission-lines diagnostics.

It is a known problem that different calibrations yield different metallicity values for individual HII regions. The galaxy where we can use most of the available calibrations is J0126-0038 (see Tab. 1). As we can see in Table 1 , the metallicities vary by more than 1 dex between the different calibrators and this happens on a similar scale for all HII regions in our sample, a similar result has also been found by Kewley & Ellison (2008) for sample of 27,730 star-forming galaxies from SDSS DR 4.

This is the case for all HII regions in our sample and seems to be a systematic offset in most cases, again as found by Kewley & Ellison (2008). Those authors tried to unify the different measurements from different lines and provide a way to convert all metallicities into the same calibration basis. We implemented this conversion method into our code using as a base metallicity KD02–N2O2 (Bianco *et al.* (2016)). The results obtained from this recalibration vary only within 0.1 dex in each HII region. We studied metallicities in different HII regions within each galaxy. In our sample the total oxygen abundance of individual HII regions is (12+log10(O/H))=8.1 ±0.15 dex in all galaxies, however in five out of seven galaxies we detect at least one or two HII regions with metallicities close to solar.

https://doi.org/10.1017/S1743921318007135 Published online by Cambridge University Press

Table 1. Comparison of different metallicity calculations for two HII regions of SDSS J012646.11-003838.8. For references to the different calibrators we refer to Bianco *et al.* (2016)

	12+log10(O/H)	12+log10(O/H)
Calibrator	**HII-1**	**HII-2**
D02	$8.033^{+0.176}_{-0.202}$	$8.120^{+0.197}_{-0.326}$
Z94	$8.488^{+0.035}_{-0.033}$	$8.759^{+0.038}_{-0.051}$
M91	$8.118^{+0.054}_{-0.045}$	$7.965^{+0.738}_{-0.053}$
PP04–N2Ha	$8.084^{+0.042}_{-0.071}$	$8.133^{+0.083}_{-0.152}$
PP04–O3N2	$8.027^{+0.040}_{-0.058}$	$8.138^{+0.075}_{-0.124}$
P10–ONS	$8.850^{+0.047}_{-0.079}$	$8.272^{+0.102}_{-0.130}$
P10–ON	$7.963^{+0.138}_{-0.220}$	$7.625^{+0.242}_{-0.310}$
M08–N2Ha	$8.102^{+0.097}_{-0.153}$	$8.268^{+0.422}_{-0.342}$
M08–O3O2	$8.364^{+0.014}_{-0.012}$	$8.590^{+0.015}_{-0.016}$
M13–O3N2	$8.063^{+0.030}_{-0.042}$	$8.138^{+0.051}_{-0.085}$
M13–N2	$8.052^{+0.066}_{-0.085}$	$8.104^{+0.112}_{-0.174}$
KD02–N2O2	$7.663^{+0.640}_{-0.111}$	$8.410^{+0.154}_{-0.808}$
KK04–N2Ha	$8.249^{+0.122}_{-0.030}$	$8.393^{+0.145}_{-0.189}$
KK04–R23	$8.312^{+0.045}_{-0.037}$	$8.172^{+0.690}_{-0.044}$
KD02comb	$8.215^{+0.050}_{-0.041}$	$8.054^{+0.453}_{-0.037}$

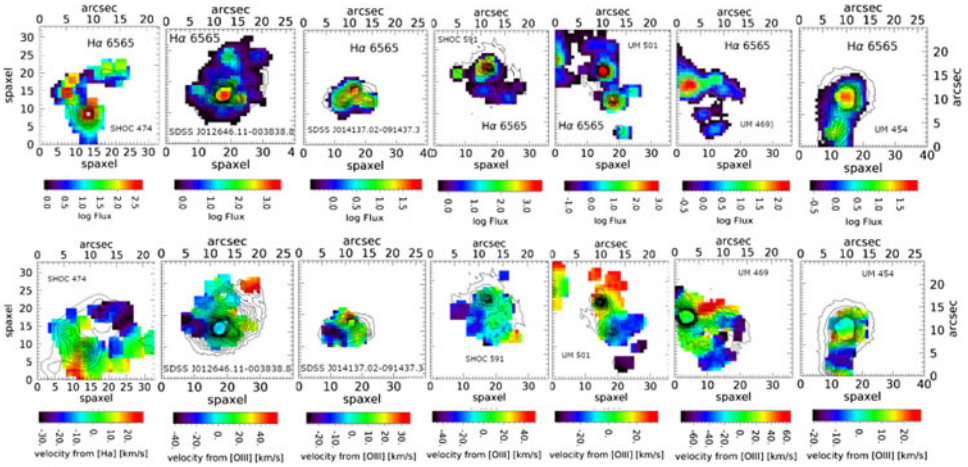

Figure 1. Maps of Hα (top) and maps of velocity (bottom) determined from Hα or OII emission lines of the seven galaxies of our sample.

3.2. *Resolved Maps*

Morphology, SFR, EW. All of our galaxies are metal-poor dwarf irregulars. They have multiple star-forming regions of different sizes surrounded by emission that extends beyond bright star-forming regions of the galaxy. Different morphologies might suggest different processes influencing the evolution of these galaxies. In Fig. 1 (top) we show Hα maps of the entire sample. SDSS J012646.11-003838.8 shows an extended structure with only one central bright star-forming region while in SDSS J014137.02-091437.3 we observe three star-forming knots in a compact galaxy. Two galaxies show conspicuous features of diffuse gas in arcs and tails outside the main galaxy, that could be signs of a recent merger. An extended jet-like structure is visible in the map of Hα UM 454 while the UM 469 Hα map shows two star-forming knots followed by pronounced arcs.

We use the luminosity of Hα as a tracer of the SFR using the relation of (Kennicutt, Tamblyn, & Congdon 1994). In our sample we measure SFRs up to 4 $M_\odot$ year^{-1} for

https://doi.org/10.1017/S1743921318007135 Published online by Cambridge University Press

individual star-forming regions. The EW maps, obtained from Hα corrected for underlying absorption, show values ranging from 50 to 800 Å. The highest values are observed at the centres of star-forming regions and they correlate with the maps of SF indicating a very young age for the most intense SF regions.

Kinematics. We obtain the kinematics of the emitting gas by fitting the line profile of Hα with a single Gaussian. The complexity of the kinematics observed in our sample can be seen in Fig. 1 (bottom). We see clear rotational patterns in UM 501, and possibly in SDSS J014137.02-091437.3, SDSS J012646.11-003838.8 and SHOC 591. The other galaxies show no clear velocity gradient nor an ordered rotation pattern. In UM 469 and SHOC 474 we observe a small feature of gas moving in our direction in the northern and southwestern part. UM 454 has rather complicated kinematics that need further study. In our sample we observe typical maximum velocities of the gas in the galaxies between 20 and 40 km/s with the exception of UM 469 where the gas reaches a velocity of 60 km/s.

References

Abazajian, K., Adelman-McCarthy, J. K., Agüeros, M. A. *et al.* 2005, *AJ*, 129, 1755
Bianco, F. B., Modjaz, M., Oh, S. M., Fierroz, D. *et al.* 2016, *AaC*, 16, 54
Bradamante, F., Matteucci, F., & D'Ercole, A. 1998, *A&A*, 337, 338
Cowie, L. L., Songaila, A., Hu, E. M., & Cohen, J. G. 1996, *AJ*, 112, 839
Davies, J. I., & Phillipps, S. 1988, *MNRAS*, 233, 553
Dohm-Palmer, R. C., Skillman, E. D., Mateo, M. *et al.* 2002, *AJ*, 123, 813
Dohm-Palmer, R. C., Skillman, E. D., Gallagher, J. *et al.* 1998, *AJ*, 116, 1227
Kennicutt, R. C., Jr., Tamblyn, P., & Congdon, C. E. 1994, *ApJ*, 435, 22
Kewley, L. J., & Ellison, S. L. 2008, *ApJ*, 681, 1183
Le Févre, O., Saisse, M., Mancini, D. *et al.* 2003, *SPIE*, 4841, 1670
Martín-Manjón, M. L., Mollá, M., Daz, A. I., & Terlevich, R. 2012, *MNRAS*, 420, 1294
Mateo, M. L. 1998, *ARA&A*, 36,435
Papaderos, P., Loose, H.-H., Thuan, T. X., & Fricke, K. J. 1996, *A&AS*, 120, 207
Sánchez, S. F., Rosales-Ortega, F. F., Marino, R. A. *et al.* 2012, *A&A*, 546, 2
Seiden, P. E., Schulman, L. S., & Gerola, H. 1979, *ApJ*, 232, 702
Tolstoy, E., Hill, V., & Tosi, M. 2009, *ARAA*, 47, 371

https://doi.org/10.1017/S1743921318007135 Published online by Cambridge University Press